NANO LETTERS

pubs.acs.org/NanoLett Letter

Graphene Strain-Effect Transistor with Colossal ON/OFF Current Ratio Enabled by Reversible Nanocrack Formation in Metal Electrodes on Piezoelectric Substrates

Yikai Zheng,[#] Dipanjan Sen,[#] Sarbashis Das, and Saptarshi Das*

Cite This: *Nano Lett.* 2023, 23, 2536−2543 Read Online

ACCESS | Metrics & More | Article Recommendations | Supporting Information

ABSTRACT: Extraordinarily high carrier mobility in graphene has led to many remarkable discoveries in physics and at the same time invoked great interest in graphene-based electronic devices and sensors. However, the poor ON/OFF current ratio observed in graphene field-effect transistors has stymied its use in many applications. Here, we introduce a graphene strain-effect transistor (GSET) with a colossal ON/OFF current ratio in excess of 10^7 by exploiting strain-induced reversible nanocrack formation in the source/drain metal contacts with the help of a piezoelectric gate stack. GSETs also exhibit steep switching with a subthreshold swing (SS) < 1 mV/decade averaged over ∼6 orders of magnitude change in the source-to-drain current for both electron and hole branch amidst a finite hysteresis window. We also demonstrate high device yield and strain endurance for GSETs. We believe that GSETs can significantly expand the application space for graphene-based technologies beyond what is currently envisioned.

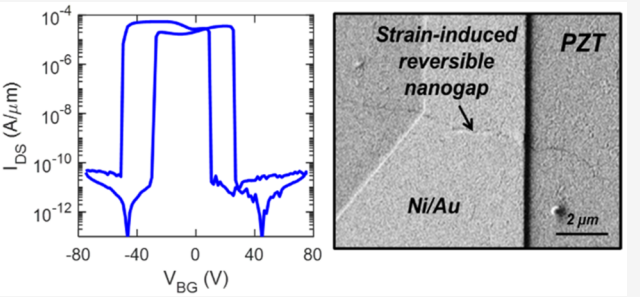

KEYWORDS: *Graphene, Straintronics, Transistor, High ON/OFF current ratio*

Graphene exhibits extraordinary electronic properties, with its electron mobility at room temperature reaching as high as 2.5 × 10^5 cm^2 V^{-1} s^{-1}[1−4] As a consequence, graphene is considered to be an excellent material for radio frequency (RF) electronics. Scaled graphene field-effect transistors (GFETs) have demonstrated cutoff frequencies in the range of several hundreds of GHz.[5] Graphene also exhibits extraordinary mechanical properties; the Young's modulus of graphene can be as high as 2.45 TPa.[8] As a result, graphene-based flexible and stretchable electronic devices have received significant attention in recent years. Graphene is also considered a promising material for smart electronic devices capable of sensing, storage, compute, security, and energy-harvesting.[9−13] Finally, exotic electronic properties, such as superconductivity, ferromagnetism, etc., have also been found in bilayer graphene with twisted stacking order.[14,15]

While the extraordinary material properties of graphene make it appealing for many applications, GFETs are hampered by their poor ON/OFF current ratio (in the range of 2−10), which can be attributed to the lack of a finite bandgap in graphene. Bulk semiconducting materials such as silicon and emerging two-dimensional (2D) semiconductors such as molybdenum disulfide offer bandgaps in the range of 1−2 eV that translate into adequate ON/OFF current ratios (in excess of 10^6) when employed as the channel material in field-effect transistors. To overcome this challenge, several approaches have been investigated to achieve a high ON/OFF current ratio in GFETs. For example, quantum confinement in graphene nanoribbons can lead to the opening of a finite bandgap,[4,6,7,16] which can be translated into an ON/OFF current ratio of ∼10^3 in GFETs.[1,4] GFETs with high-k gate dielectrics such as ferroelectric barium titanate can also demonstrate ON/OFF current ratios of ∼10^4.[17] Electrochemical modification of the graphene channel through the use of electrolyte gating with honey, organic liquids, etc., can also lead to ON/OFF current ratios exceeding 10^8 in GFETs, albeit with limited yield and relatively poor endurance.[20,21] Finally, vertical heterostructure designs of graphene with other semiconducting materials (Si, Ge, WS_2) have reported ON/OFF current ratios as high as ∼10^6.[18,19,22,23]

Here, we introduce a novel straintronic approach to achieve colossal ON/OFF current ratios (>10^7) in GFETs at room temperature without compromising the high transconductance offered by the graphene channel. We harness strain-induced reversible cracking in high tensile strength source/drain metal contacts to graphene as the switching mechanism in graphene

Received: November 16, 2022
Revised: February 22, 2023
Published: March 30, 2023

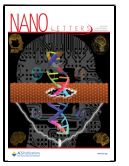

https://doi.org/10.1021/acs.nanolett.2c04519
Nano Lett. 2023, 23, 2536−2543

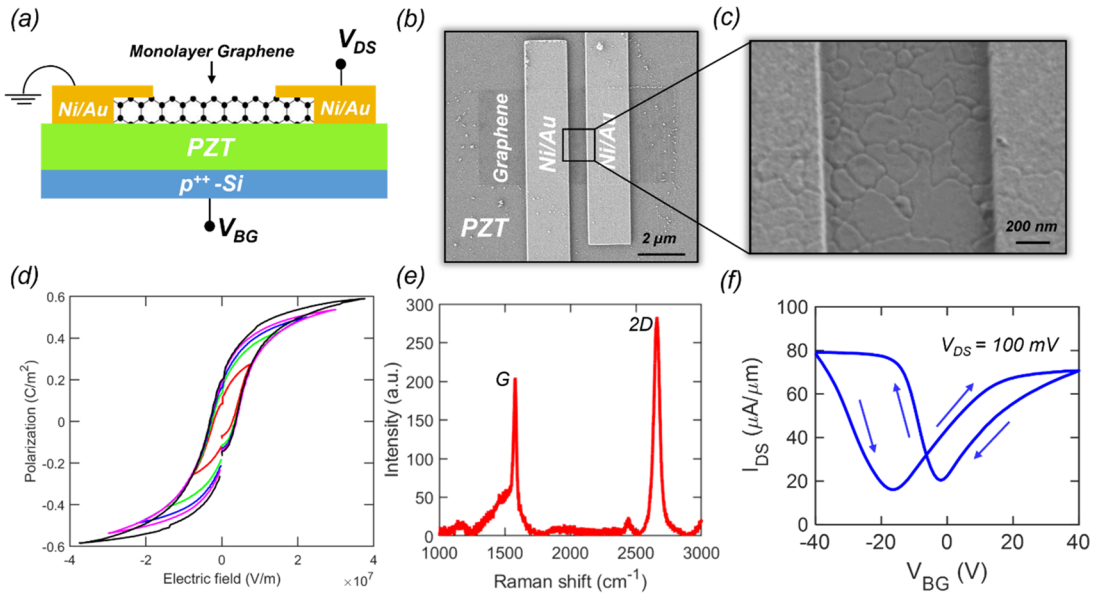

Figure 1. Characterization of the graphene strain-effect transistors (GSETs). (a) 2D schematic and (b) scanning electron microscope (SEM) image of a representative GSET on a 2 μm thick PZT film, grown on a p^{++}-Si substrate, with Ni/Au as the source/drain contacts. The channel length and width for the GSET were 1 and 5 μm, respectively. (c) Top-view SEM image of the PZT film with columnar grain structure. (d) Nested polarization versus electric field hysteresis loops measured for the PZT film using a metal−insulator−metal (MIM) structure. A remnant polarization of 0.2 C/m^2 and a coercive field of 2 × 10^6 V/m can be extracted. (e) Raman spectra of a representative monolayer graphene channel obtained using a 532 nm laser. (f) Transfer characteristics, i.e., source-to-drain current (I_{DS}) versus back-gate voltage (V_{BG}), of a representative as-fabricated GSET measured under room temperature at a source-to-drain voltage (V_{DS}) of 100 mV.

strain-effect transistors (GSETs). We also utilize piezoelectric lead zirconate titanate (PZT) as a gate dielectric to transduce gate voltage into strain for dynamic strain engineering in metal contacts to graphene. We demonstrate strain-induced abrupt switching across 50 GSETs with a mean ON/OFF current ratio of >10^6, a high transconductance of >100 μS/μm, and a subthreshold swing (SS) of <1 mV/decade with a finite hysteresis window.

Figure 1a−b, respectively, shows the 2D schematic and a scanning electron microscope (SEM) image of a GSET. A 2 μm thick film of piezoelectric lead zirconate titanate (PZT) was used as the back-gate dielectric. The PZT film was grown on a p^{++}-Si substrate using the sol−gel method with a [110] crystal orientation. 0.4 M $PbNb_{0.2}(Zr_{0.52}Ti_{0.48})_{0.98}O_3$ sol gel with a 10 mol % Pb excess was used since it is near the morphotropic phase boundary (MPB), i.e., the boundary between the tetragonal and rhombohedral phases, in the $PbTiO_3/PbZrO_3$ solid solution.[24,26] At this composition, the piezoelectric and dielectric properties are significantly enhanced.[25,27] A ∼2 mol % Nb dopant concentration also serves to improve the piezoelectric and dielectric properties.[28] Figure 1c shows an enhanced top-view SEM image of the PZT film with columnar grain structure. Separate metal−insulator−metal (MIM) structures were fabricated to characterize the PZT film. Figure 1d shows the nested polarization versus electric field hysteresis loops of the PZT film, with a remnant polarization of 0.2 C/m^2 and a coercive field of 2 × 10^6 V/m. These "minor loops" and accompanying saturation loop are common for most ferroelectric materials and are ascribed to partial switching of ferroelectric domains when the applied electric field across the film is smaller than the coercive field.[30−32] We found the highest saturation polarization value to be ∼0.6 C/m^2 at an applied voltage of 80 V for the 2 μm-thick PZT substrate. A dual beam laser interferometer was used to measure the d_{33} coefficient of the unpoled PZT film. A "clamped" value of ∼50 pm/V was extracted. A Ni strain gauge was also fabricated to calibrate the in-plane strain as a function of applied bias to the PZT film; a maximum strain value of ∼0.25% was extracted for a 50 V bias across the PZT film.

Next, a commercially available, chemical vapor deposition (CVD) grown large-area monolayer graphene film was transferred onto the PZT substrate using a wet transfer technique.[33] Graphene channels were defined by electron beam lithography (EBL) and oxygen plasma etching. The source/drain contacts were also patterned using EBL followed by electron beam evaporation of Ni/Au and a standard lift-off process. The choice of Ni as the contact metal was motivated by its high-tensile strength,[20,34] which is critical for observing large current ON/OFF ratios in GSETs. Electrical and optical characterization were performed to assess the as-fabricated GSETs. Figure 1e shows the Raman spectra obtained using a 532 nm laser on a representative graphene channel, with two characteristic peaks at around 1600 and 2700 cm^{-1}. The peak at ∼1600 cm^{-1} is the G band, which appears prominently in sp^2-hybridized carbon materials such as graphene. The other peak at ∼2700 cm^{-1} is the 2D band (also known as the G' band), which confirms that the graphene utilized in this study is monolayer. Figure 1f shows the transfer characteristics, i.e., source-to-drain current (I_{DS}) versus back-gate voltage (V_{BG}), of a representative as-fabricated GSET, measured under room temperature at a source-to-drain voltage (V_{DS}) of 100 mV. The channel length and width for the GSET were 1 and 5 μm, respectively. The ambipolar transfer characteristics can be attributed to the lack of bandgap in graphene, which allows seamless injection of electrons and holes into their respective transport bands from the source/drain metal contacts. The clockwise hysteresis observed in the transfer characteristics can be attributed to physiosorbed and chemisorbed molecules at the graphene/PZT interface originating from one or more sources, including metal contaminants introduced by the

https://doi.org/10.1021/acs.nanolett.2c04519
Nano Lett. 2023, 23, 2536−2543

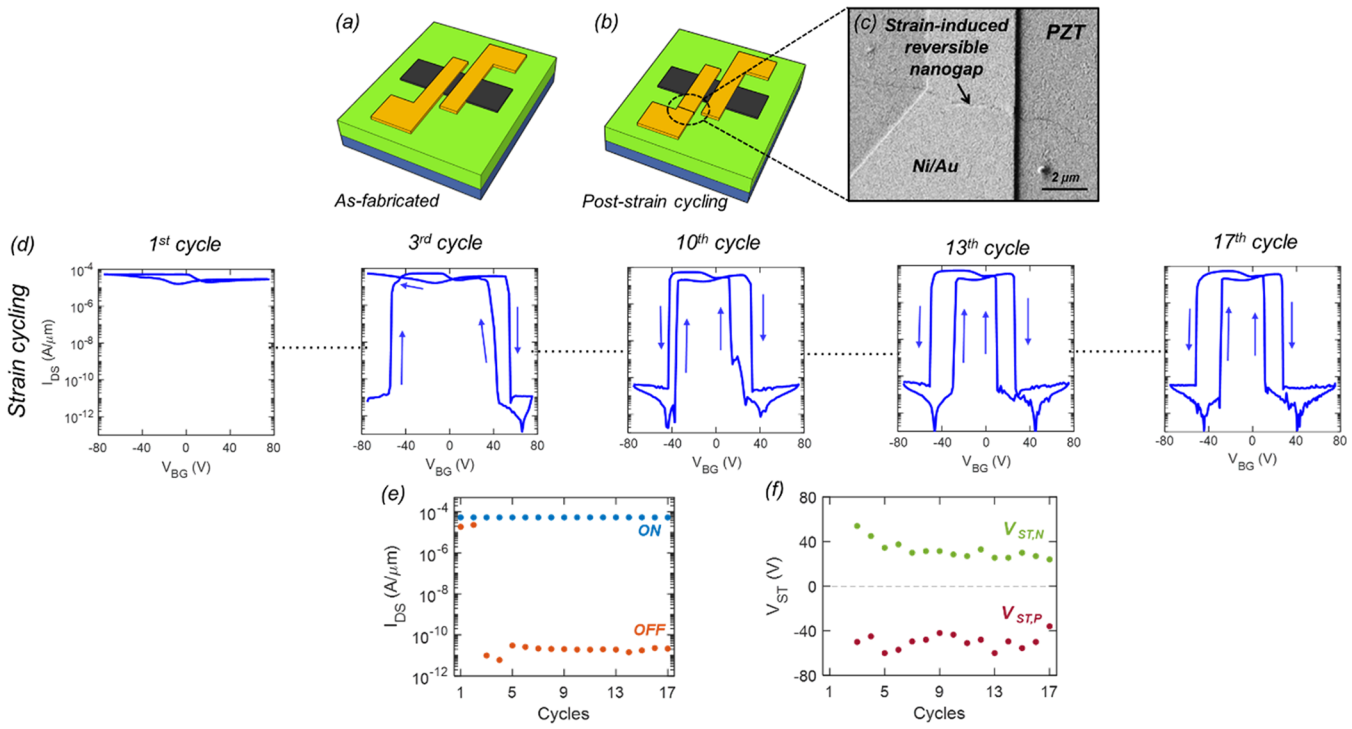

Figure 2. Strain cycling in a GSET leading to colossal ON/OFF current ratio. 3D schematic diagrams of (a) an as-fabricated GSET and (b) a postforming GSET. Following a strain cycling forming process, a nanogap develops across the metal contact of the GSET. (c) A zoomed-in SEM image of the GSET clearly shows the existence of a nanogap across the metal contact, which is responsible for the abrupt drop in conductance of the device. (d) Overview of a 17 strain cycling process in the representative GSET; forming occurs at the 3rd cycle and a high ON/OFF current ratio is retained for all subsequent strain cycles. The corresponding (e) ON/OFF current ratio and (f) switching threshold voltages ($V_{ST,P}$ and $V_{ST,N}$) of the 17 strain cycles. Clearly, the switching behavior occurs after the 2nd strain cycle. The ON/OFF current ratio, as well as $V_{ST,P}$ and $V_{ST,N}$, stabilizes over the subsequent strain cycles.

copper etchant chemistry, as well as polymer residues and defects introduced by the graphene transfer and fabrication processes.[11,12] Furthermore, the negative shift in the Dirac voltage, i.e., the gate voltage at which I_{DS} is minimum, during the forward sweep indicates unintentional p-type doping of the graphene channel. The electron and hole mobility values, extracted from peak transconductance at V_{BG} = 2 V and V_{BG} = −9 V, were found to be 128 $cm^2\ V^{-1}\ s^{-1}$ and 375 $cm^2\ V^{-1}\ s^{-1}$, respectively. The maximum current ON/OFF ratio for the electron and hole branches were extracted to be ∼3.5 and ∼3.8, respectively.

As expected, the transfer characteristics of the as-fabricated GSET do not demonstrate a large ON/OFF current ratio. However, when the PZT film is subjected to repeated strain cycling by applying V_{BG}, electrically reversible crack formation takes place in the metal contacts to graphene, which restricts current conduction through the device and leads to colossal ON/OFF current ratio in the excess of 10^7 in the GSET. Figure 2a−c, respectively, shows the 3D schematics and a zoomed-in SEM image of a representative GSET with a nanogap introduced in the Ni/Au contact after voltage-induced strain cycling in the PZT. We refer to this process as forming. Figure 2d shows the evolution of the transfer characteristics (taken in the logarithmic scale) of a GSET during the forming process, i.e., as a function of the strain cycling for the first 10 V_{BG} sweeps from −75 to 75 V, and over an additional 7 cycles when measured using a V_{DS} of 100 mV. Note that, in contrast to traditional ambipolar characteristics, i.e., ON−OFF−ON, GSETs demonstrate antiambipolar characteristics, i.e., OFF−ON−OFF; this is due to the fundamentally different operating principle of the GSET that involves strain-induced switching between the ON and OFF states. Also note that the nanoscale crack at the electrodes forms and disrupts the current transport when the magnitude of the back gate voltage (V_{BG}) exceeds the respective switching thresholds for both negative and positive biases, i.e., $V_{ST,P}$ and $V_{ST,N}$, respectively, resulting in an OFF-state for our GSETs when $V_{BG} < V_{ST,P}$ and $V_{BG} > V_{ST,N}$. However, when $V_{ST,P} < V_{BG} < V_{ST,N}$, the reversible nanoscale crack at the electrode is sealed and the current transport path is recovered, placing the device in the ON-state.

Figure 2e−f shows the trend of ON/OFF current ratio and switching threshold voltages ($V_{ST,P}$ and $V_{ST,N}$), respectively, across 17 strain cycles. The switching behavior initially appears for both negative and positive V_{BG} after the second strain cycle; the ON/OFF current ratio as well as $V_{ST,P}$ and $V_{ST,N}$ further stabilize over subsequent strain cycles. Supporting Information Figure 1 illustrates the full 17 strain cycling process of a representative GSET. The postformed GSET maintains a high ON-state current owing to the high carrier mobility of graphene while at the same time offering a large current ON/OFF ratio $>10^7$. As stated previously, the reversible cracking in the metal contacts occurs for both positive and negative V_{BG}, leading to large current ON/OFF ratios for both electron and hole branches. The switching thresholds (V_{ST}) for the17th GSET measurement cycle in Figure 2d were found to be −32 ± 10 V and −48 ± 8 V for the hole branch and 28 ± 3 V and 11 ± 2 V for the electron branch during the forward and reverse sweeps, respectively. The hysteresis observed in the transfer characteristics can be explained from the fact that

https://doi.org/10.1021/acs.nanolett.2c04519
Nano Lett. 2023, 23, 2536−2543

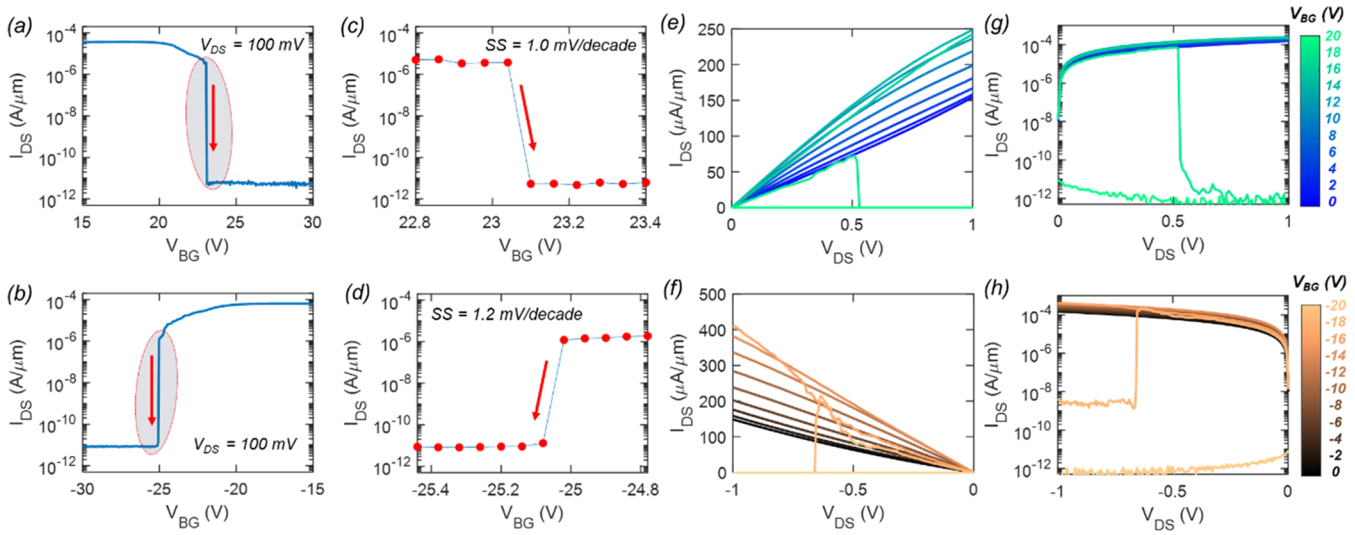

Figure 3. Steep switching in GSETs. Transfer characteristics of a representative postformed GSET showing steep switching in the (a) electron branch and (b) hole branch. Zoomed-in transfer characteristics near the abrupt switching region reveals (c) SS = 1.0 mV/decade for the electron and (d) SS = 1.2 mV/decade for the hole branch. The extracted SS value is limited by the step size of 6 mV used for sweeping the V_{BG}. Output characteristics, i.e., I_{DS} versus V_{DS}, at different V_{BG} of the GSET for the (e) electron branch and (f) hole branch in the linear scale and (g) electron branch and (h) hole branch in the logarithmic scale. In the ON-state, i.e., $|V_{BG}| < |V_{ST,P}|$ and $|V_{BG}| < |V_{ST,N}|$, the GSET exhibits linear output characteristics owing to the semimetallic nature of graphene.

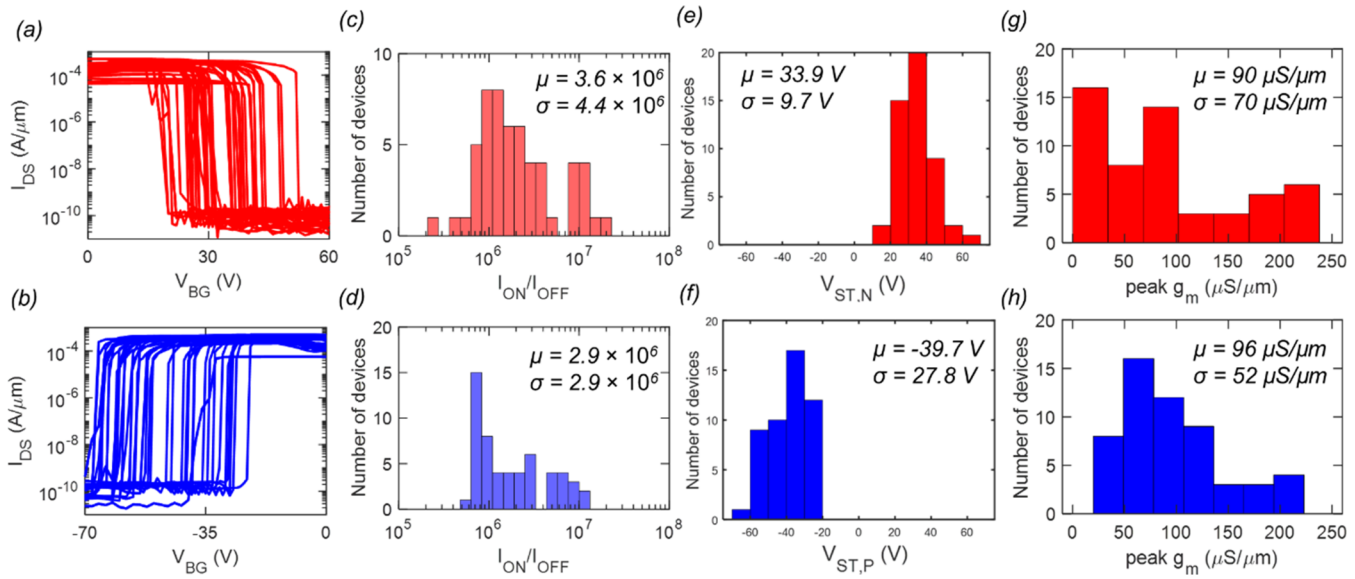

Figure 4. Statistical evaluation of GSETs. Transfer characteristics of 50 GSETs for (a) the electron branch and (b) the hole branch. Distribution of ON/OFF current ratios for (c) electron branch and (d) hole branch. The mean values of the ON/OFF current ratio were found to be 3.6×10^6 for the electron branch and 2.9×10^6 for the hole branch, which can meet the requirements for most logic applications. Distribution of (e) $V_{ST,N}$ and (f) $V_{ST,P}$. The mean and standard deviation values for $V_{ST,N}$ were found to be 33.9 and 9.7 V for the electron branch. The mean and standard deviation values for $V_{ST,P}$ were found to be −39.7 V and 27.8 V for the hole branch. The mean value for $V_{ST,N}$ and $V_{ST,P}$ can be reduced by utilizing a thinner PZT back-gate substrate. Distribution of g_m for (g) electron branch and (h) hole branch. The mean and standard deviation values for g_m were found to be 90 μS/μm and 70 μS/μm for the electron branch and 96 μS/μm and 52 μS/μm for the hole branch, respectively. These g_m values are at par with most state-of-the-art amplifiers.

piezoelectric thin films do not switch uniformly but rather through the motion of domain walls that are often pinned at surface defects. This results in a highly nonuniform strain distribution across the piezoelectric domains and leads to asymmetric in-plane tensile/compressive strains with respect to the applied electric field. In GSETs, this leads to hysteresis in the switching behavior: a larger magnitude of V_{BG} opens the crack and a smaller magnitude of V_{BG} closes the crack.

The cycle-to-cycle variation in the transfer characteristics of a representative GSET (see Supporting Information Figure 2) can also be ascribed to the same phenomenon. Nevertheless, once the cracks are formed through strain cycling, the opening and closing of the cracks are highly reproducible as demonstrated by the constant ON/OFF current ratio obtained following the second strain cycle in Figure 2e and by the endurance measurements in Supporting Information Figure 3. The variation of $V_{ST,P}$ and $V_{ST,N}$ for the same representative

https://doi.org/10.1021/acs.nanolett.2c04519
Nano Lett. 2023, 23, 2536−2543

GSET is shown in Figure 2f. Such variation in the switching voltages is the result of strain-induced reversible cracking in the high-tensile strength source/drain metal contacts to graphene.

Figure 3a–b shows the transfer characteristics of a representative GSET (postforming), and Figure 3c–d shows the same transfer characteristics zoomed-in near V_{ST} for the electron and hole branches, respectively, when measured with a step size of 6 mV. The switching between the ON and the OFF states was found to be abrupt with a subthreshold swing (SS) of ∼1.0 mV/decade and 1.2 mV/decade averaged over ∼6 orders of magnitude change in I_{DS} for the electron and hole branches, respectively. Note that the extracted SS value is limited by the step size of 6 mV used for sweeping the V_{BG} (see Supporting Information Figure 4 for demonstrations of steep switching in 10 additional GSETs). Also note that conventional metal-oxide-semiconductor field-effect transistors (MOSFETs) are thermodynamically limited to a minimum SS of 60 mV/decade, which is referred to as the Boltzmann tyranny.[35] Alternative device concepts such as the tunnel field-effect transistors (TFETs) can achieve steep slope switching. However, there are only a handful of experimental demonstrations (<25) with sub-60 mV/decade SS.[36−43] TFETs also suffer from low ON-state currents due to band-to-band tunneling limitations.[44] Negative capacitance field-effect transistors (NCFETs) exploit a ferroelectric gate-stack to achieve steep slope switching without compromising ON-state performance.[45−49] However, material and interface non-idealities can significantly impact the performance of NCFETs, including the desired SS of less than 60 mV/decade, and the concept of negative capacitance is still under active debate.[50,51] In this context, GSETs can offer an alternative solution for achieving low SS values, though the previously discussed hysteresis window would likely need to be reduced for practical implementation. Figure 3e–h shows the output characteristics, i.e., I_{DS} versus V_{DS}, of the same GSET at different V_{BG} for the electron/hole branches and in linear and logarithmic scales, respectively. In the ON-state, i.e., $|V_{BG}| < |V_{ST,N}|$ and $|V_{BG}| < |V_{ST,P}|$, the GSET exhibits linear output characteristics owing to the semimetallic nature of graphene.

Figure 4a–b shows the transfer characteristics of 50 GSETs for the electron and the hole branches, respectively. Figure 4c–h shows the distributions of current ON/OFF ratio, $V_{ST,P}$, $V_{ST,N}$, and peak transconductance (g_m) for the electron and the hole branches extracted from these same 50 GSETs, respectively. The mean and standard deviation values for the ON/OFF current ratio were found to be 3.6×10^6 and 4.4×10^6 for the electron branch and 2.9×10^6 and 2.9×10^6 for the hole branch, respectively. In other words, most GSETs offer an ON/OFF current ratio $>10^6$ for both electron and hole branches when V_{DS} = 100 mV. The device-to-device variation in V_{ST} can be attributed to the random distribution of domains on the PZT substrate. The mean and standard deviation values for V_{ST} were found to be 33.9 and 9.7 V for $V_{ST,N}$ and −39.7 V and 27.8 V for $V_{ST,P}$, respectively.

Note that the mean of $V_{ST,N}$ and $V_{ST,P}$ can be reduced by utilizing a thinner PZT substrate as the back-gate, which is also attractive for eventual device miniaturization and reduction in back-gate operating voltage. Nevertheless, strain cycling leads to reproducible GSETs with large ON/OFF current ratios and abrupt switching without compromising the high ON-current and transconductance values offered by graphene. The mean and standard deviation values for the transconductance (g_m) were found to be 90 $\mu S/\mu m$ and 70 $\mu S/\mu m$ for the electron branch and 96 $\mu S/\mu m$ and 52 $\mu S/\mu m$ for the hole branch, respectively. The large deviation in transconductance is attributed to device-to-device variation across the 50 GSETs stemming from variations in impurity concentration introduced from transfer and fabrication processes as well as surface defects at the domain walls of the PZT substrate.[11]

Finally, we have benchmarked the key figure of merit of the GSET, i.e., the current ON/OFF ratio, against other approaches as shown in Table 1. We found that our straintronic approach offers greater current ON/OFF ratios as compared to GFETs based on graphene nanoribbons that are aided by finite bandgap opening due to quantum confinement and, at the same time, eliminates fabrication challenges associated with nanopatterning of graphene, such as edge nonuniformity. GSETs also offer better yield and are more reliable/reproducible compared to electrochemical GFETs that rely on hydrogenation reactions involving liquid-gate dielectrics. In addition, the device structure and fabrication of GSETs are significantly simpler than that of vertical heterostructures while also offering higher current ON/OFF ratios. Nanoelectromechanical (NEM) transistors and switches,[52−54] as well as strain-based devices,[55] can also achieve high ON/OFF current ratios, though they lack the high transconductance demonstrated in our GSET devices.

Table 1. Benchmarking Table of I_{ON}/I_{OFF} for State-of-the-Art Graphene Transistors

Mechanism	V_{DS} (V)	I_{ON}/I_{OFF}	ref
Quantum Confinement	0.5	2×10^3	1
	0.005	1.1×10^3	4
	−5	10^4	6
	−0.1	14	7
Heterostructures	0.2	10^4	18
	2	$>10^6$	19
	1	10^8	24
	2	10^5	23
	0.1	10^6	22
	29	10^6	25
Hydrogenation	0.05	$>10^4$	29
	0.5	10^8	20
Strain-effect	**0.1**	**$>10^7$**	**this work**

In conclusion, we have demonstrated an alternative approach to realize large ON/OFF current ratios ($>10^6$) in a GFET by harnessing strain-induced reversible crack formation in the source/drain metal contacts with the help of a piezoelectric gate stack. We have also demonstrated ultra-steep slope switching with a subthreshold swing (SS) of <1 mV/decade averaged over 6 orders of magnitude change in the source-to-drain current in GSETs for both electron and hole branches. Finally, GSETs are easy to fabricate, offer high yield, and can endure a large number of strain cycles, making them a promising technology for steep-slope graphene devices with large ON/OFF current ratios.

METHODS

Fabrication of PZT Film. The PZT film we used in our work was grown by chemical solution deposition (CSD) method.[56−58] Adapted from previously established procedures,[26] a composition of 0.4 M $PbNb_{0.2}(Zr_{0.52}Ti_{0.48})_{0.98}O_3$ sol gel with a 10 mol % Pb excess was prepared and deposited on platinized wafers. The sol–gel solution contains Zr, Ti, Nb,

https://doi.org/10.1021/acs.nanolett.2c04519
Nano Lett. 2023, 23, 2536−2543

and Pb organic precursors dissolved in 2-methoxyethanol (2-MOE) along with an acetylacetone chelating agent. The PZT films are deposited on a platinized Si wafer ($Pt(111)/TiO_2/SiO_2/Si$). An oxidized Si wafer is used to prevent the formation of a Pt silicide. A 30 nm Ti layer is sputtered and then oxidized at 700 °C for 15 min in O_2 in a rapid thermal annealing (RTA) tool. Next, a $PbTiO_3$ seed layer is deposited using layer-by-layer process: each layer is ∼80 nm and a total of 25 layers were deposited to achieve a total thickness of 2.02 ± 0.03 μm.

Transfer of Monolayer Graphene. CVD-grown graphene on a Cu foil was purchased from ACS material (GFCU0101) and spin-coated with poly(methyl methacrylate) (PMMA). The Cu/graphene/PMMA stack was then placed in a copper etchant (iron III chloride) until the Cu was completely etched. The graphene/PMMA film was rinsed in three consecutive deionized water baths for 10 min each to wash away excess metal ions. The film was subsequently transferred onto the fabrication substrate and baked for 10 min at 150 °C. Then to further improve the adhesion between graphene and PZT substrate without degradation of piezoelectric property of the substrate due to thermal annealing, the transferred sample was kept in circulating air for 24 h, efficiently removing water molecules between graphene and PZT substrate. Finally, PMMA was removed using acetone and isopropyl alcohol, leaving behind the graphene film on the substrate.

Fabrication of the GSET. The fabrication of the GSET has two fabrication steps. The first is to define graphene channel region with oxygen plasma etch method. To define the source and drain contacts, sample is then spin coated with methyl methacrylate (MMA) followed by A3 PMMA. Then using e-beam lithography source and drain contacts are patterned and developed by using 1:1 mixture of MIBK and IPA for 60s. 40 nm of Nickel (Ni) and 30 nm of Gold (Au) are deposited using e-beam evaporation. Finally, the lift-off process is performed to remove the evaporated Ni/Au except from the source/drain patterns by immersing the sample in acetone for 30 min, followed by IPA for another 30 min.

Scanning Electron Microscopy (SEM). Scanning electron microscopy (SEM) of the GSETs used in this study was conducted using a Zeiss Merlin field emission scanning electron microscopy (FESEM) system at an accelerating voltage of 1 kV.

Electrical Characterization. Electrical characterization of the fabricated devices are performed using Lake Shore CRX-VF probe station under atmospheric pressure using a Keysight B1500A parameter analyzer.

■ ASSOCIATED CONTENT

Data Availability Statement

The data sets generated during and/or analyzed during the current study are available from the corresponding author on reasonable request.

Supporting Information

The Supporting Information is available free of charge at https://pubs.acs.org/doi/10.1021/acs.nanolett.2c04519.

Transfer characteristics for total 17 strain cycling, cycle-to-cycle variation, and endurance for one GSET, and statistics for 10 GSETs (PDF)

Accession Codes

The codes used for plotting the data are available from the corresponding authors on reasonable request.

■ AUTHOR INFORMATION

Corresponding Author

Saptarshi Das − *Department of Engineering Science and Mechanics, Penn State University, University Park, Pennsylvania 16802, United States; Department of Electrical Engineering, Department of Materials Science and Engineering, and Materials Research Institute, Penn State University, University Park, Pennsylvania 16802, United States;* orcid.org/0000-0002-0188-945X; Email: sud70@psu.edu

Authors

Yikai Zheng − *Department of Engineering Science and Mechanics, Penn State University, University Park, Pennsylvania 16802, United States*

Dipanjan Sen − *Department of Engineering Science and Mechanics, Penn State University, University Park, Pennsylvania 16802, United States*

Sarbashis Das − *Department of Electrical Engineering, Penn State University, University Park, Pennsylvania 16802, United States*

Complete contact information is available at: https://pubs.acs.org/10.1021/acs.nanolett.2c04519

Author Contributions

#Equal contributions

Notes

The authors declare no competing financial interest.

■ ACKNOWLEDGMENTS

The work was supported by the National Science Foundation (NSF) through CAREER Award under Grant Number ECCS-2042154.

■ REFERENCES

(1) Dragoman, M.; Dinescu, A.; Dragoman, D. Room temperature nanostructured graphene transistor with high ON/OFF ratio. *Nanotechnology* **2017**, *28* (1), 015201.

(2) Mayorov, A. S.; et al. Micrometer-scale ballistic transport in encapsulated graphene at room temperature. *Nano Lett.* **2011**, *11* (6), 2396−9.

(3) Novoselov, K. S.; Fal'ko, V. I.; Colombo, L.; Gellert, P. R.; Schwab, M. G.; Kim, K. A roadmap for graphene. *Nature* **2012**, *490* (7419), 192−200.

(4) Lu, Y.; Goldsmith, B.; Strachan, D. R.; Lim, J. H.; Luo, Z.; Johnson, A. T. C. High-On/Off-Ratio Graphene Nanoconstriction Field-Effect Transistor. *Small* **2010**, *6* (23), 2748−2754.

(5) Wu, Y.; et al. High-frequency, scaled graphene transistors on diamond-like carbon. *Nature* **2011**, *472* (7341), 74−78.

(6) Jeong, B.; Wuttke, M.; Zhou, Y.; Müllen, K.; Narita, A.; Asadi, K. Graphene Nanoribbon Field-Effect Transistors with Top-Gate Polymer Dielectrics. *ACS Appl. Electron. Mater.* **2022**, *4* (6), 2667−2671.

(7) Bai, J.; Zhong, X.; Jiang, S.; Huang, Y.; Duan, X. Graphene nanomesh. *Nat. Nanotechnol* **2010**, *5* (3), 190−4.

(8) Lee, J.-U.; Yoon, D.; Cheong, H. Estimation of Young's modulus of graphene by Raman spectroscopy. *Nano Lett.* **2012**, *12* (9), 4444−4448.

(9) Jang, H.; Park, Y. J.; Chen, X.; Das, T.; Kim, M. S.; Ahn, J. H. Graphene-based flexible and stretchable electronics. *Adv. Mater.* **2016**, *28* (22), 4184−4202.

(10) Akinwande, D.; Petrone, N.; Hone, J. Two-dimensional flexible nanoelectronics. *Nat. Commun.* **2014**, *5* (1), 5678.

(11) Dodda, A.; Subbulakshmi Radhakrishnan, S.; Schranghamer, T. F.; Buzzell, D.; Sengupta, P.; Das, S. Graphene-based physically

unclonable functions that are reconfigurable and resilient to machine learning attacks. *Nat. Electron.* **2021**, *4*, 364−374.
(12) Schranghamer, T. F.; Oberoi, A.; Das, S. Graphene memristive synapses for high precision neuromorphic computing. *Nat. Commun.* **2020**, *11* (1), 5474.
(13) Huang, H.; et al. Graphene-Based Sensors for Human Health Monitoring. *Front Chem.* **2019**, *7*, 399.
(14) Yankowitz, M.; et al. Tuning superconductivity in twisted bilayer graphene. *Science* **2019**, *363* (6431), 1059−1064.
(15) Sharpe, A. L.; et al. Emergent ferromagnetism near three-quarters filling in twisted bilayer graphene. *Science* **2019**, *365* (6453), 605−608.
(16) Han, M. Y.; Özyilmaz, B.; Zhang, Y.; Kim, P. Energy band-gap engineering of graphene nanoribbons. *Physical Review Letters* **2007**, *98* (20), 206805.
(17) Alam, I.; et al. Graphene field-effect transistor using gated ferroelectric thin film. *Solid State Commun.* **2021**, *340*, 114533.
(18) Britnell, L.; et al. Field-effect tunneling transistor based on vertical graphene heterostructures. *Science* **2012**, *335* (6071), 947−50.
(19) Strobel, C.; et al. Novel Graphene Adjustable-Barrier Transistor with Ultra-High Current Gain. *ACS Appl. Mater. Interfaces* **2022**, *14* (34), 39249−39254.
(20) Li, S. R.; et al. Large transport gap modulation in graphene via electric-field-controlled reversible hydrogenation. *Nat. Electron.* **2021**, *4* (4), 254−260.
(21) Hayashi, C. K.; Garmire, D. G.; Yamauchi, T. J.; Torres, C. M.; Ordonez, R. C. High on-off ratio graphene switch via electrical double layer gating. *IEEE Access* **2020**, *8*, 92314−92321.
(22) Bai, Z.; et al. Highly Tunable Carrier Tunneling in Vertical Graphene-WS(2)-Graphene van der Waals Heterostructures. *ACS Nano* **2022**, *16* (5), 7880−7889.
(23) Wu, H.; et al. Multifunctional Half-Floating-Gate Field-Effect Transistor Based on MoS(2)-BN-Graphene van der Waals Heterostructures. *Nano Lett.* **2022**, *22* (6), 2328−2333.
(24) Schneider, D. S.; et al. MoS_2/graphene Lateral Heterostructure Field Effect Transistors. In *2021 Device Research Conference (DRC)*, 20−23 June 2021; pp 1−2. DOI: 10.1109/DRC52342.2021.9467156.
(25) Lee, J. H.; et al. Semiconductor-less vertical transistor with I_{ON}/I_{OFF} of 10^6. *Nat. Commun.* **2021**, *12* (1), 1000.
(26) Wolf, R. A.; Trolier-McKinstry, S. Temperature dependence of the piezoelectric response in lead zirconate titanate films. *J. Appl. Phys.* **2004**, *95* (3), 1397−1406.
(27) Karapuzha, A. S.; James, N. K.; Khanbareh, H.; van der Zwaag, S.; Groen, W. A. Structure dielectric and piezoelectric properties of donor doped PZT ceramics across the phase diagram. *Ferroelectrics* **2016**, *504* (1), 160−171.
(28) Kayasu, V.; Ozenbas, M. The effect of Nb doping on dielectric and ferroelectric properties of PZT thin films prepared by solution deposition. *J. Eur. Ceram. Soc.* **2009**, *29* (6), 1157−1163.
(29) Hayashi, C. K.; Garmire, D. G.; Yamauchi, T. J.; Torres, C. M.; Ordonez, R. C. High on-off ratio graphene switch via electrical double layer gating. *IEEE Access* **2020**, *8*, 1−1.
(30) Yimnirun, R.; Wongmaneerung, R.; Wongsaenmai, S.; Ngamjarurojana, A.; Ananta, S.; Laosiritaworn, Y. Dynamic hysteresis and scaling behavior of hard lead zirconate titanate bulk ceramics. *Appl. Phys. Lett.* **2007**, *90* (11), 112908.
(31) Wang, C.-M.; Lau, K.; Wang, Q. Dynamic hysteresis and scaling behaviours of lead-free 0.94 $Bi_{0.5}Na_{0.5}TiO_3$−0.06$BaTiO_3$ bulk ceramics. *RSC Adv.* **2016**, *6* (36), 30148−30153.
(32) Tsang, C.; Wong, C.; Shin, F. Modeling saturated and unsaturated ferroelectric hysteresis loops: An analytical approach. *J. Appl. Phys.* **2005**, *98* (8), 084103.
(33) Schranghamer, T. F.; Sharma, M.; Singh, R.; Das, S. Review and comparison of layer transfer methods for two-dimensional materials for emerging applications. *Chem. Soc. Rev.* **2021**, *50* (19), 11032−11054.
(34) Hou, W.; et al. Strain-based room-temperature non-volatile MoTe2 ferroelectric phase change transistor. *Nat. Nanotechnol.* **2019**, *14* (7), 668−673.
(35) Meindl, J. D.; Chen, Q.; Davis, J. A. Limits on silicon nanoelectronics for terascale integration. *Science* **2001**, *293* (5537), 2044−2049.
(36) Ionescu, A. M.; Riel, H. Tunnel field-effect transistors as energy-efficient electronic switches. *Nature* **2011**, *479* (7373), 329−37.
(37) Appenzeller, J.; Lin, Y. M.; Knoch, J.; Avouris, P. Band-to-Band Tunneling in Carbon Nanotube Field-Effect Transistors. *Phys. Rev. Lett.* **2004**, *93* (19), 196805.
(38) Choi, W. Y.; Park, B.-G.; Lee, J. D.; King Liu, T.-J. Tunneling field-effect transistors (TFETs) with subthreshold swing (SS) less than 60 mV/dec. *Ieee Electr Device L* **2007**, *28* (8), 743−745.
(39) Borg, B. M.; Dick, K. A.; Ganjipour, B.; Pistol, M.-E.; Wernersson, L.-E.; Thelander, C. InAs/GaSb heterostructure nanowires for tunnel field-effect transistors. *Nano Lett.* **2010**, *10* (10), 4080−4085.
(40) Ganjipour, B.; Wallentin, J.; Borgstrom, M. T.; Samuelson, L.; Thelander, C. Tunnel field-effect transistors based on InP-GaAs heterostructure nanowires. *ACS Nano* **2012**, *6* (4), 3109−3113.
(41) Sarkar, D.; et al. A subthermionic tunnel field-effect transistor with an atomically thin channel. *Nature* **2015**, *526* (7571), 91−95.
(42) Wu, P.; et al. Complementary Black Phosphorus Tunneling Field-Effect Transistors. *ACS Nano* **2019**, *13* (1), 377−385.
(43) Wu, P.; Appenzeller, J. Reconfigurable Black Phosphorus Vertical Tunneling Field-Effect Transistor With Record High ON-Currents. *IEEE Electron Device Lett.* **2019**, *40* (6), 981−984.
(44) Cristoloveanu, S.; Wan, J.; Zaslavsky, A. A Review of Sharp-Switching Devices for Ultra-Low Power Applications. *IEEE Journal of the Electron Devices Society* **2016**, *4* (5), 215−226.
(45) Salahuddin, S.; Datta, S. Use of Negative Capacitance to Provide Voltage Amplification for Low Power Nanoscale Devices. *Nano Lett.* **2008**, *8* (2), 405−410.
(46) Ko, E.; Lee, J. W.; Shin, C. Negative Capacitance FinFET With Sub-20-mV/decade Subthreshold Slope and Minimal Hysteresis of 0.48 V. *IEEE Electron Device Lett.* **2017**, *38* (4), 418−421.
(47) Lee, M. H.; et al. Physical thickness 1.x nm ferroelectric HfZrOx negative capacitance FETs. *2016 IEEE International Electron Devices Meeting (IEDM)* **2016**, 12.1.1−12.1.4.
(48) Cheema, S. S.; et al. Enhanced ferroelectricity in ultrathin films grown directly on silicon. *Nature* **2020**, *580* (7804), 478−482.
(49) Si, M.; et al. Sub-60 mV/dec ferroelectric HZO MoS_2 negative capacitance field-effect transistor with internal metal gate: The role of parasitic capacitance. *2017 IEEE International Electron Devices Meeting (IEDM)* **2017**, 23.5.1−23.5.4.
(50) Cao, W.; Banerjee, K. Is negative capacitance FET a steep-slope logic switch? *Nat. Commun.* **2020**, *11* (1), 196.
(51) Alam, M. A.; Si, M.; Ye, P. D. A critical review of recent progress on negative capacitance field-effect transistors. *Appl. Phys. Lett.* **2019**, *114* (9), 090401.
(52) Lee, J. O.; et al. A sub-1-V nanoelectromechanical switching device. *Nat. Nanotechnol* **2013**, *8* (1), 36−40.
(53) Zaghloul, U.; Piazza, G. Sub-1-V Piezoelectric Nanoelectromechanical Relays With Millivolt Switching Capability. *IEEE Electron Device Lett.* **2014**, *35* (6), 669−671.
(54) Kim, J. H.; Chen, Z. C.; Kwon, S.; Xiang, J. Three-terminal nanoelectromechanical field effect transistor with abrupt subthreshold slope. *Nano Lett.* **2014**, *14* (3), 1687−91.
(55) Guan, Y.; Guo, Z.; You, L. Ferroelectric Nanogap-Based Steep-Slope Ambipolar Transistor. *Small* **2022**, *18* (48), No. e2203017.
(56) Schwartz, R. W. Chemical Solution Deposition of Perovskite Thin Films. *Chem. Mater.* **1997**, *9* (11), 2325−2340.
(57) Budd, K. D.; Dey, S. K.; Payne, D. A. Sol−Gel Processing OF PbTiO//3, PbZrO//3, PZT, and PLZT Thin Films. *British Ceramic Proceedings* **1985**, 107−121.
(58) Schulman, D. S. Contact, Interface, and Strain Engineering of Two-Dimensional Transition Metal Dichalcogenide Field Effect

https://doi.org/10.1021/acs.nanolett.2c04519
Nano Lett. 2023, 23, 2536−2543

Transistors, Ph.D. Thesis, The Pennsylvania State University, Ann Arbor, 2019.

https://doi.org/10.1021/acs.nanolett.2c04519
Nano Lett. 2023, 23, 2536−2543